Synthesis and magnetic properties of Ni–BaTiO3 nanocable arrays within ordered anodic alumina templates

David Sallagoïty, Catherine Elissalde, Jérôme Majimel, Romain Berthelot, U-Chan Chung Seu, Nicolas Penin, Mario Maglione, Vlad Antohe, Gaël Hamoir, Flavio Abreu Araujo, et al.

Synthesis and magnetic properties of Ni–BaTiO3 nanocable arrays within ordered anodic alumina templates

Sallagoity D.[1,2], Elissalde C.[1], Majimel J.[1], Berthelot R.[3], Chung Seu U.-C.[1], Penin N.[1], Maglione M.[1], Antohe V. A.[2], Hamoir G.[2], Abreu Araujo F.[2], Piraux L.[2]

1/ CNRS, Univ. Bordeaux, ICMCB, UPR 9048, 87 Avenue du Docteur Schweitzer, 33600 Pessac, France
2/ Institute of Condensed Matter and Nanosciences, Université catholique de Louvain, Place Croix du Sud, B-1348, Louvain-la-Neuve, Belgium
3/ ICGM-UMR5253, Université Montpellier II, 2 Place Eugène Bataillon, CC 1502, 34095 Montpellier CEDEX 5, France

Abstract :

A reliable and flexible synthesis route was used for processing high density Ni–$BaTiO_3$ nanocable arrays based on wet chemical impregnation and subsequent electrodeposition within a highly ordered unidirectional porous alumina membrane. The core–shell structure was carefully investigated by bright field scanning transmission electronic microscopy coupled with energy dispersive X-ray spectroscopy. The strength of the dipolar interaction arising from the packing density of the magnetic nanowires was correlated with the $BaTiO_3$ wall thickness through magnetometry and ferromagnetic resonance measurements. Our approach opens a pathway to obtain optimized nanostructured multiferroic composites exhibiting tunable magnetic properties.

1. Introduction

One-dimensional magnetic nanostructures have been paid great attention in different research fields due to their unique properties and their possible exploitation in relevant applications, such as patterned media for magnetic storage,[1,2] non-reciprocal microwave devices,[3–5] spintronic devices[6–9] and biomedicine.[10,11] To tailor the physical properties of 1D nanostructures to a more diverse range, heterostructures that combine two or more materials with different magnetic and electric properties in a radial structure open new perspectives towards the elaboration of multiferroic composite materials. In this regard, the coexistence and coupling between the ferromagnetic and ferroelectric properties may lead to the attractive electric control of the magnetic properties. Tuning the properties of such ferromagnetic core nanowires (NWs) through their interactions with the ferroelectric shell is of interest for developing microwave devices and metamaterial structures with enhanced electrical tunability of their operating frequency.[12,13]

Multiferroic composites consisting of arrays of magnetic nanowires surrounded by a ferroelectric material have been synthesized using various methods, such as sputtering,[12] electrospinning[14,15] and template assisted growth techniques.[16–20] There is growing interest in the use of template synthesis due to its flexibility and reliability performances. Only a few studies along this line involved a combination of wet impregnation and electrodeposition to elaborate core–shell nanocables comprising a ferromagnetic metal[20] or oxide[18] core surrounded by a dielectric oxide shell in anodic aluminium oxide (AAO) nanoporous membranes. The versatility of this approach lies in the tunability of the nanocable length, the core diameter, the ferroelectric tube wall thickness, and consequently the packing density of the magnetic nanowires. However a detailed structural and morphological study is not yet reported. Well-designed coaxial heterostructures are required to achieve desired properties and functionalities.

In this work, we used the combination of wet chemical oxide impregnation and subsequent metal electrodeposition processes in AAO to elaborate a high density array of coaxial nanocables, made of Ni ferromagnetic nanowires surrounded by $BaTiO_3$ (BTO) dielectric nanotubes (NTs). We propose a complete description of our Ni–BTO nanocomposites using

electron microscopy and magnetic characterization using Superconducting Quantum Interference Device (SQUID) and Ferromagnetic Resonance (FMR) measurements. We investigate the influence of the wall thickness of the BTO NTs on the magnetic properties of the coaxial nanocable arrays.

2. Experimental section

Commercial AAO templates (Synkera Technology Inc., Longmont, CO, USA) were used as the host membrane. These membranes have narrow pore distribution and excellent thermal and chemical stabilities. Arrays of pure Ni NWs have been fabricated by direct electrodeposition in AAO membranes having a thickness of 50 µm with a pore diameter of 150 nm, an inter-pore distance (the center to center distance between pores) of 210–220 nm and a porosity (P) of 30%. The system used is a three-electrode system with Pt foil as the anode electrode and an Ag/AgCl electrode as the reference electrode. A Cu layer was evaporated on one side of the membrane in order to cover the pores and use it as a cathode. Ni NWs were grown at a constant potential of −1.1 V vs. Ag/AgCl from a 1 M $NiSO_4 \cdot 6H_2O$ + 0.5 M H_3BO_3 electrolyte at ambient temperature. The plating current is recorded as a function of time and the electrodeposition process is stopped before the wires emerge from the surface, as evidenced by a sudden increase of the plating current.

Arrays of Ni–BTO nanocables were elaborated using a multi-step process consisting of sol–gel impregnation, thermal annealing and crystallisation of BTO NTs followed by Ni electrodeposition within the pore walls of the AAO templates coated with BTO (see Scheme 1).

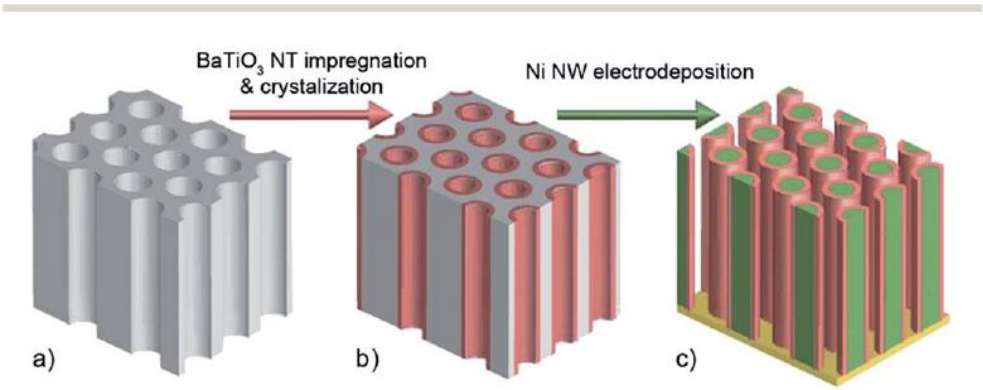

Scheme 1 Ni–$BaTiO_3$ nanocable multistep synthesis.

The BT sol was synthesized using barium acetate $Ba(CH_3CO_2)_2$ and titanium(IV) isopropoxide $Ti(OCH(CH_3)_2)_4$ from Sigma Aldrich as precursors.[21] Subsequently, $Ba(OAc)_2$ was dissolved in glacial acetic acid at 80 °C under magnetic stirring. Titanium was dissolved in a second vessel containing isopropanol at room temperature under stirring. Then the two solutions were mixed under stirring at room temperature to form an homogeneous 0.4 M stoichiometric BT sol. AAO templates were immersed into the BT sol for one minute. Wet faces were carefully dried with absorbant paper to remove the BT film formed on the top, before the crystallization annealing. The calcination temperature was also strictly limited to 700 °C in order to avoid membrane film curvature and the phase transformation of amorphous alumina into α-Al_2O_3 (onset at 860 °C as shown by thermal analysis). These points are crucial but rarely underlined in the literature: such an alumina crystallization has detrimental effects for several reasons: (i) it can affect the BTO microstructure through surface rearrangement and interdiffusion across interfaces and (ii) only amorphous alumina can be completely removed in NaOH to allow an unambiguous characterization of the BTO nanotubes,[22] and the membrane film curvature prevents the subsequent Ni electrodeposition into the AAO templates coated with BTO from occurring. The uniform growth of the Ni nanowires was stopped before the nanowires reach the surface of the AAO template to preserve the one-dimensional

core–shell shape. Ferromagnetic resonance (FMR) measurements at room temperature have been done in the field swept mode using a microstrip transmission line with an external magnetic field applied parallel to the revolution axis, as reported previously for NWs within porous templates.[23] Room temperature magnetometry measurements were performed using a Quantum Design SQUID Magnetometer.

3. Results and discussion

SEM investigations (10 kV) were first carried out to check the BTO NT structure after the removal of the alumina template with 1 M NaOH (aq) solution (see Fig. 1(a)). A bundle of thin NTs with a high aspect ratio is formed driven by strong interactions between the hydrophilic surfaces of adjacent BTO NTs. Holes and asperities are identified on the surface of the NTs.

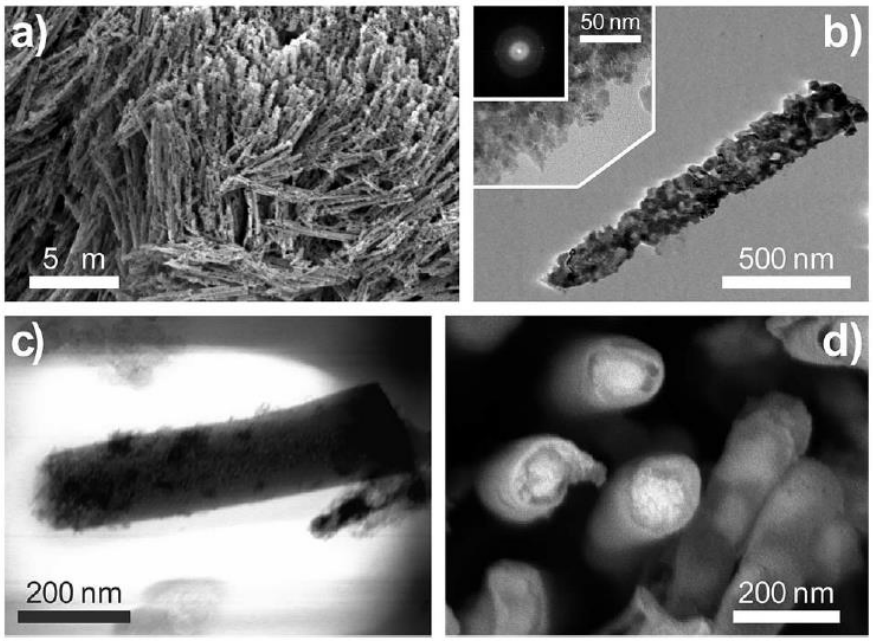

Fig. 1 (a) SEM picture of the $BaTiO_3$ nanotube bundle after the removal of the alumina template. (b) HRTEM micrograph of a fractured nanotube (zoom on individual crystallites with a digital diffractogram illustrating the polycrystalline organization in the inset). (c) HRTEM micrograph of a single Ni nanowire. (d) SEM image of Ni–$BaTiO_3$ core–shell nanocables.

It can be explained by the partial dissolution of barium species during the etching process (Ba-rich well-defined micrometric hexagonal objects can appear when the NaOH concentration is higher than 1 M). TEM measurements (200 kV) were performed after the template removal and ultrasonic dispersion in ethanol (see Fig. 1(b)). The BTO NTs collected are usually broken into several segments with lengths of a few micrometers. They consist of fine-grained polycrystalline materials with a compact texture as confirmed by the diffraction pattern exhibiting a series of concentric rings (see the inset in Fig. 1(b)). The BTO NTs have grain sizes in the range of 20–30 nm and grains have no preferential orientation with respect to the tube axis. Ni NWs with a few micrometers in length were also observed by HRTEM (see Fig. 1(c)). The

electrodeposited Ni NWs appear as nanometer-sized (5–10 nm) polycrystalline materials with no preferential orientation along the wire axis. This is confirmed by XRD measurements (not shown) in agreement with a previous study on electrodeposited Ni NWs.[24] The polycrystalline nature of the Ni NWs with small grains is also evidenced by the high resolution SEM image of core–shell NWs shown in Fig. 1(d). The diameter of the metallic core is about 90–100 nm, while the thickness of the shell is 20–30 nm.

Bright field scanning transmission electron microscopy (STEM) experiments coupled with Energy Dispersive X-ray Spectroscopy (EDX) analyses were performed on Ni–BTO core–shell nanowires after grinding and dispersion in ethanol (Fig. 2(a) and (b)). EDX profiles across Ba, Ti and Ni rich areas (Fig. 2(c)) can be compared with the total projected thickness of a nanotube along the direction of the electron beam (t) which is described by the following eqn:

$$t = \sqrt{r_0{}^2 - r^2} - \sqrt{r_i{}^2 - r^2}; \quad r < r_i \qquad (1)$$

$$t = \sqrt{r_0{}^2 - r^2}; \quad r < r_i \qquad (2)$$

where r_0 and r_i represent the outer and the inner radii of the BTO tubes, respectively. The experimental data are found to be in good agreement with the calculated profile that confirms the nanotube shape of BTO. In contrast, the Ni chemical profile exhibits a single maximum in the core region of the BTO tube which reveals clearly the core–shell structure. The mean tube wall thickness is about 30 nm in agreement with the crystallite size estimated in Fig. 1(b) and the core diameter is close to 90 nm. The core–shell morphology is also confirmed from the EDS mapping performed on isolated Ni–$BaTiO_3$ NWs, as shown in Fig. 2(d).

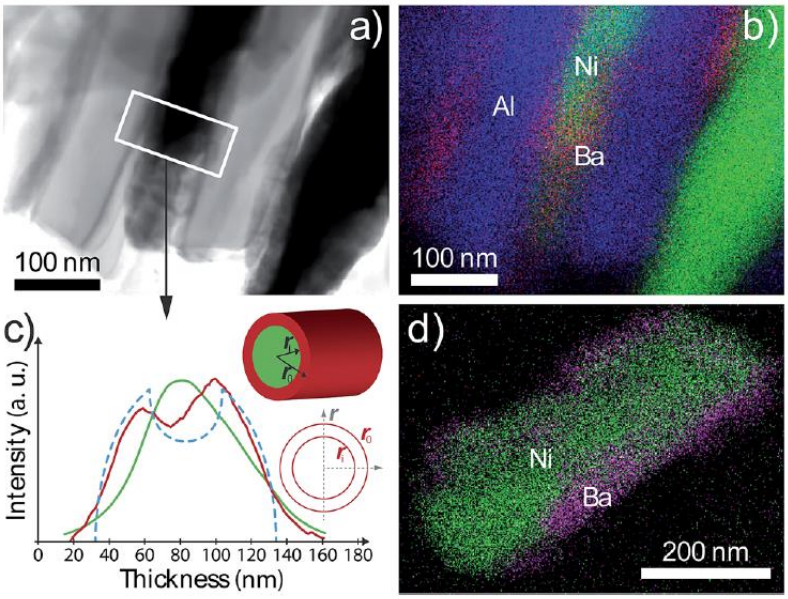

Fig. 2 (a) Bright field STEM micrograph of Ni–$BaTiO_3$ core–shell architecture within the template after grinding and dispersion in EtOH. (b) Chemical mapping of the area in (a), with Ba, Ni and Al in red, green, and blue respectively. (c) EDX profiles integrated along the marked area in (a), with (Ba and Ti) and Ni in red and green respectively; blue refers to the simulation of total BTO tube projected along the electron beam direction for a 30 nm wall thickness tube into a 150 nm diameter pore. (d) BF-STEM micrograph of an isolated Ni–$BaTiO_3$ core–shell after template removal.

For Ni NW and Ni–BTO nanocable ordered arrays within AAO, magnetocrystalline anisotropy (MCA) contributions can be neglected so the effective field H_{eff} in the saturated state contains only the shape anisotropy and the dipolar interaction field. Moreover since both nanowire systems have the same symmetry and for the samples considered here their aspect ratio is large, the same mean field model used for NWs can also be used for core–shell NWs. Therefore, the effective field can be expressed as[25]

$$H_{\text{eff}} = 2\pi M_s - 6\pi M_s P \qquad (3)$$

where $2\pi M_s$ is the shape anisotropy, $6\pi M_s P$ is the dipolar interaction field in the saturated state and M_s = 485 emu cm^{-3} is the saturation magnetization density for Ni. Due to their different volume, the packing fractions for the core–shell system (P_{Ni-BTO}) and nanowires (P_{Ni}) are different and when grown in the same template $P_{Ni-BTO} < P_{Ni}$. Fig. 3 compares the normalized hysteresis loops measured at room temperature with the field applied along the revolution axis of the NWs. A clear difference is observed between the two samples, in particular Ni–BTO core–shell NWs are more easily magnetized than their Ni NWs counterpart. The main differences observed in their hysteresis loops arise from their respective effective fields and in particular from the dipolar interaction field. Indeed, as mentioned above $P_{Ni-BTO} < P_{Ni}$, which as seen from the second term in eqn (3), results in a smaller interaction field and thus a higher effective field and a stronger uniaxial anisotropy in core–shell NWs. Moreover, the high packing values of the templates result in a strong dipolar interaction which is responsible for the shearing of the hysteresis loops and their reduced squareness. This shearing depends on the value of the dipolar interaction field and so the hysteresis loops of NWs are more sheared than those measured in core–shell NWs.[26] It is also noted that nanowire and nanocable systems exhibit similar coercive fields (around 250 Oe).

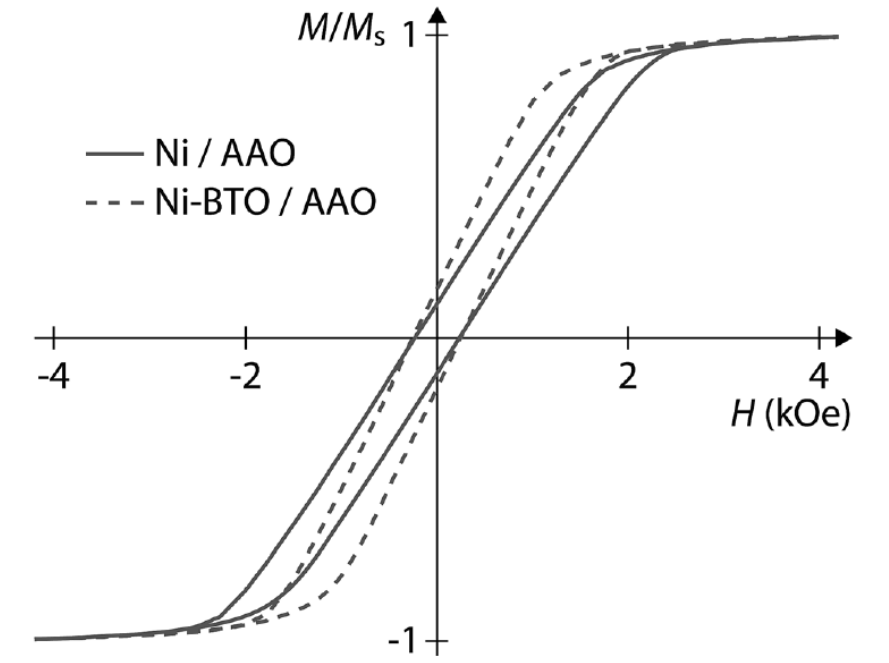

Fig. 3 Room temperature hysteresis loops measured along the revolution axis in arrays of Ni nanowires (dashed line) and of Ni–BTO nanocables (solid line) embedded in AAO templates.

In order to have an accurate determination of the effective field H_{eff}, the FMR properties of these core–shell nanowires have been measured. These magnetically filled porous membranes are particularly well adapted for a simple fabrication of the micro-strip transmission line and the investigation of the ferromagnetic resonance properties at GHz frequencies.[25,27] The microwave signal propagating along the microstrip transmission line deposited on the free surface of the membrane (Fig. 4(a)) produces a microwave pumping field which is perpendicular to the nanowires and induces a precession of the magnetization around the static equilibrium position.

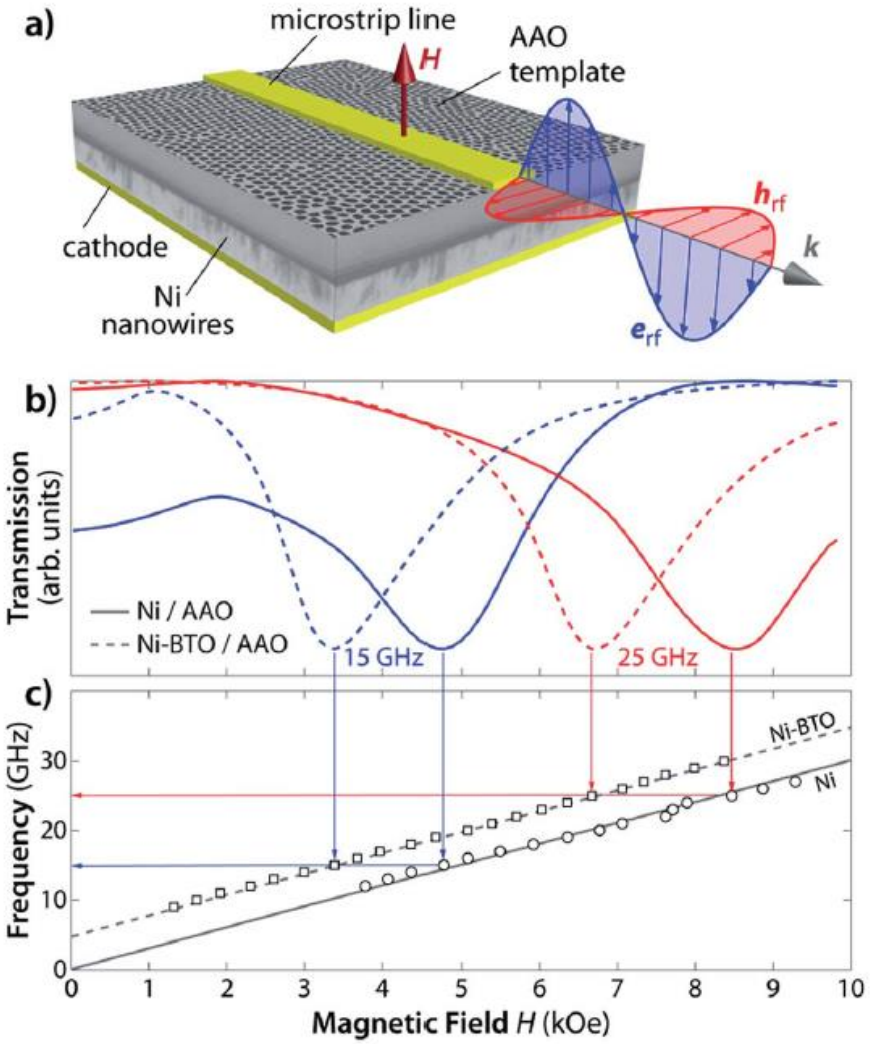

Fig. 4 (a) Schematics of the microstrip transmission line, in which the cathode, or ground plane, is separated from the 150 μm-wide microstrip line by a dielectric which corresponds to the AAO membrane containing the nanocables. (b) Field sweep microwave absorption spectra obtained at 300 K and recorded at 15 GHz and 25 GHz with the field applied parallel to the wire axis for arrays of Ni–BTO NWs and Ni NWs grown in AAO. (c) The corresponding measured dispersion relations.

At ferromagnetic resonance, power is absorbed from the incident microwave signal and the corresponding minimum in the transmitted power is recorded using a network analyzer. The analysis of the FMR results is made in the saturation state where the magnetization inside the wires can be considered as a single domain. At a given constant frequency f, the ferromagnetic resonance condition when the magnetic field is applied parallel to the wires is[25]

$$H_r = \frac{f}{\gamma} - H_{eff} \qquad (4)$$

where H_r is the resonance field and γ is the gyromagnetic ratio (γ ~3.09 GHz kOe^{-1} for Ni). Fig. 4(b) presents a set of transmission spectra obtained at room temperature and recorded at 15 GHz and 25 GHz for both Ni nanowires and Ni–BTO nanocables. From the spectra shown in Fig. 4(b), it can be observed that at the same frequency, the core–shell NW sample presents lower resonance fields than the reference Ni NW sample. The shift of the resonance field is about 1.5 kOe and a clear upward displacement of the dispersion relation of the core–shell NW sample with respect to those of the corresponding Ni NWs is observed. From eqn (4), it can be seen that at a given frequency, a decrease of the H_r resonance field corresponds to an increase of the effective field in Ni–BTO NWs which results from their lower packing fraction. Fig. 4(c) shows their corresponding dispersion relations, where the straight lines correspond to the fit of the experimental data to eqn (4). Fitting of the experimental data yields the effective field, H_{eff}, and the packing fractions for NWs and NTs in each template. For Ni NWs, we get H_{eff} ~0 kOe and P_{Ni} ~30% while for Ni–BTO core–shell NWs, we get H_{eff} ~1.4 kOe and $P_{Ni–BTO}$ ~16%. Assuming that BTO nanotubes cover homogeneously the wall of the pores, we estimate the wall thickness around 35 nm, in agreement with previous electronic microscopy observations.

4. Conclusions

In conclusion, we have reported a reliable and controllable synthesis method for high-density arrays of coaxial Ni–$BaTiO_3$ nanocables within anodic aluminium oxide membranes. This synthesis approach based on a combination of electrochemical and sol–gel processes allows for modulation of the magnetic properties of core–shell nanowires by an appropriate choice of membrane material, packing fraction, geometric parameters (i.e., core radius and shell thickness) and composition. The detailed investigation of the structural and morphological features of these metal/oxide nanocables is an important step towards the elaboration of one-dimensional multiferroic nanostructures with rigorously tailored architectures. Distorted magnetic hysteresis loops and shifted ferromagnetic resonances are in agreement with the decreased packing of Ni wires in the core–shell nanocables as compared to the nanowires. Further work is under progress to achieve enhanced magnetic/electrical tunability of their properties which is of considerable importance for developing tunable microwave devices and new metamaterial structures.

Acknowledgements

F.A.A. acknowledges the Research Science Foundation of Belgium (FRS-FNRS) for financial support (FRIA grant). The IDS FunMat European doctoral school is acknowledged for financial support.

Notes and References

1. C. A. Ross, Patterned magnetic recording media, Annu. Rev. Mater. Res., 2001, 31, 203–235
2. D. Sellmyer, Y. Xu, M. Yan, Y. Sui, J. Zhou and R. Skomski, Assembly of High-Anisotropy $L1_0$ FePt Nanocomposite Films, J. Magn. Magn. Mater., 2006, 303, 302–308
3. J. F. Allaeys, B. Marcilhac and J. C. Mage, Influence of track-etching on polycarbonate membrane permittivity, J. Phys. D: Appl. Phys., 2007, 40, 3714
4. M. Darques, J. De La Torre Medina, L. Piraux, L. Cagnon and I. Huynen, Microwave Circulator Based on Ferromagnetic Nanowire in an Alumina Template, Nanotechnology, 2010, 21, 145208
5. C. E. Carreon-Gonzalez, J. De La Torre Medina, L. Piraux and A. Encinas, Electrodeposition Growth of Nanowire Arrays with Height Gradient Profiles for Microwave Device Applications, Nano Lett., 2011, 11, 2023–2027

6. L. Piraux, K. Renard, R. Guillemet, S. Matefi-Tempfli, M. Matefi-Tempfli, V. A. Antohe, S. Fusil, K. Bouzehouane and V. Cros, Template-Grown NiFe/Cu/NiFe Nanowires for Spin Transfer Devices, Nano Lett., 2007, 7, 2563–2567
7. N. Biziere, E. Mure and J. P. Ansermet, Microwave Spin-Torque Excitation in a Template-Synthesized Nanomagnet, Phys. Rev. B: Condens. Matter Mater. Phys., 2009, 79, 012404
8. D. Pullini, D. Busquets Mataix and A. Tommasi, Nanowires Implementations and Applications, ed. Abbass Hashim, 2011, pp. 223–244, InTech, ISBN 978-953-307-318-7
9. F. Abreu Araujo, M. Darques, K. A. Zvezdin, A. V. Khvalkovskiy, N. Locatelli, K. Bouzehouane, V. Cros and L. Piraux, Microwave Signal Emission in Spin-Torque Vortex Oscillators in Metallic Nanowires: Experimental Measurements and Micromagnetic Numerical Study, Phys. Rev. B: Condens. Matter Mater. Phys., 2012, 86, 064424
10. A. Hultgren, M. Tanase, E. J. Felton, K. Bhadriraju, A. K. Salem, C. S. Chen and D. H. Reich, Optimization of Yield in Magnetic Cell Separations Using Nickel Nanowires of Different Lengths, Biotechnol. Prog., 2005, 21, 509–515
11. Y. Sun, L. Hao, C. L. Chien and P. C. Searson, Tuning the Properties of Magnetic Nanowires, IBM J. Res. Dev., 2005, 49, 79–102
12. H. Zheng, J. Wang, S. E. Lofland, Z. Ma, L. Mohaddes-Ardabili, T. Zhao, L. Salamanca-Riba, S. R. Shinde, S. B. Ogale, F. Bai, D. Viehland, Y. Jia, D. G. Schlom, M. Wuttig, A. Roytburd and R. Ramesh, Multiferroic $BaTiO_3$–$CoFe_2O_4$ Nanostructures, Science, 2004, 303, 661–663
13. J. Ma, J. Hu, Z. Li and C. W. Nan, Recent Progress in Multiferroic Magnetoelectric Composites: from Bulk to Thin Films, Adv. Mater., 2011, 23, 1062–1087
14. F. Yao, L. Xu, B. Lin and G. D. Fuet, Preparation and Applications of Functional Nanofibers Based on the Combination of Electrospinning, Controlled Radical Polymerization and Click Chemistry, Nanoscale, 2010, 2, 1348–1357
15. S. Xie, F. Ma, Y. Liu and J. Li, Multiferroic $CoFe_2O_4$–$Pb(Zr_{0.52}Ti_{0.48})O_3$ Core–Shell Nanofibers and their Magnetoelectric Coupling, Nanoscale, 2011, 3, 3152–3158
16. X. L. Liu, M. Y. Li, Z. Q. Hu, Y. D. Zhu, S. Dong and X. Z. Zhao, Preparation and Properties of the $CoFe_2O_4/Bi_{3.15}Nd_{0.85}Ti_3O_{12}$ Multiferroic Composite Coaxial Nanotubes, Mater. Lett., 2012, 82, 57–60
17. X. L. Liu, M. Y. Li, J. Wang, Z. Q. Hu, Y. D. Zhu and X. Z. Zhao, Preparation and Characterization of Multiferroic $CoFe_2O_4/Bi_{0.97}Ce_{0.03}FeO_3$ Coaxial Nanotubes, Appl. Phys. A, 2012, 108, 829–834
18. M. Liu, X. Li, H. Imrane, Y. Chen, T. Goodrich, Z. Cai, K. S. Ziemer, J. Y. Huang and N. X. Sun, Synthesis of Ordered Arrays of Multiferroic $NiFe_2O_4$–$Pb(Zr_{0.52}Ti_{0.48})O_3$ Core–Shell Nanowires, Appl. Phys. Lett., 2007, 90, 152501
19. S. H. Johnson, P. Finkel, O. D. Leaffer, S. S. Nonnenmann and K. Bussman, Magneto-Elastic Tuning of Ferroelectricity within a Magnetoelectric Nanowire, Appl. Phys. Lett., 2011, 99, 182901
20. T. Narayanan, B. Mandal, A. K. Tyagi, A. Kumarasiri, X. Zhan, M. G. Hahm, M. R. Anantharaman, G. Lawes and P. M. Ajayan, Hybrid Multiferroic Nanostructure with Magnetic–Dielectric Coupling, Nano Lett., 2012, 12, 3025–3030
21. A. Hernandez, K. Chang and E. Fisher, Sol–Gel Template Synthesis and Characterization of $BaTiO_3$ and $PbTiO_3$ Nanotubes, Chem. Mater., 2002, 14, 480–482
22. Z. L. Xiao, C. Y. Han, U. Welp, H. H. Wang, W. K. Kwok, G. A. Willing, J. M. Hiller, R. E. Cook, D. J. Miller and G. W. Crabtree, Fabrication of Alumina Nanotubes and Nanowires by Etching Porous Alumina Membranes, Nano Lett., 2002, 2(11), 1293–1297
23. J. De La Torre Medina, M. Darques and L. Piraux, Strong Low Temperature Magnetoelastic Effects in Template Grown Ni Nanowires, J. Phys. D: Appl. Phys., 2008, 41, 032008
24. H. Pan, B. Liu, J. Yi, C. Poh, S. Lim, J. Ding, Y. Feng, C. H. A. Huan and J. Lin, Growth of Single-Crystalline Ni and Co Nanowires via Electrochemical Deposition and Their Magnetic Properties, J. Phys. Chem. B, 2005, 109, 3094–3098
25. A. Encinas-Oropesa, M. Demand, L. Piraux, E. Huynen and U. Ebels, Dipolar Interactions in Arrays of Nickel Nanowires Studied by Ferromagnetic Resonance, Phys. Rev. B: Condens. Matter Mater. Phys., 2001, 63, 104415
26. F. Zighem, T. Maurer, F. Ott and G. Chaboussant, Dipolar Interactions in Arrays of Ferromagnetic Nanowires: a Micromagnetic Study, J. Appl. Phys., 2011, 109, 013910
27. M. Darques, A. Encinas, L. Vila and L. Piraux, Tailoring of the c-axis Orientation and Magnetic Anisotropy in Electrodeposited Co Nanowires, J. Phys.: Condens. Matter, 2004, 16, S2279